

## Near-real time retrieval of tropospheric NO<sub>2</sub> from OMI

K. F. Boersma<sup>1,\*</sup>, H. J. Eskes<sup>1</sup>, J. P. Veefkind<sup>1</sup>, E. J. Brinkma<sup>1</sup>, R. J. van der A<sup>1</sup>, M. Sneep<sup>1</sup>, G. H. J. van den Oord<sup>1</sup>, P. F. Levelt<sup>1</sup>, P. Stammes<sup>1</sup>, J. F. Gleason<sup>2</sup>, and E. J. Bucsela<sup>2</sup>

<sup>1</sup>KNMI, De Bilt, The Netherlands

<sup>2</sup>NASA GSFC, Greenbelt, MD, USA

\*now at: Harvard University, Cambridge, USA

Received: 7 November 2006 – Published in Atmos. Chem. Phys. Discuss.: 29 November 2006

Revised: 21 February 2007 – Accepted: 5 April 2007 – Published: 27 April 2007

**Abstract.** We present a new algorithm for the near-real time retrieval – within 3 h of the actual satellite measurement – of tropospheric NO<sub>2</sub> columns from the Ozone Monitoring Instrument (OMI). The retrieval is based on the combined retrieval-assimilation-modelling approach developed at KNMI for off-line tropospheric NO<sub>2</sub> from the GOME and SCIAMACHY satellite instruments. We have adapted the off-line system such that the required a priori information – profile shapes and stratospheric background NO<sub>2</sub> – is now immediately available upon arrival (within 80 min of observation) of the OMI NO<sub>2</sub> slant columns and cloud data at KNMI. Slant columns for NO<sub>2</sub> are retrieved using differential optical absorption spectroscopy (DOAS) in the 405–465 nm range. Cloud fraction and cloud pressure are provided by a new cloud retrieval algorithm that uses the absorption of the O<sub>2</sub>-O<sub>2</sub> collision complex near 477 nm. On-line availability of stratospheric slant columns and NO<sub>2</sub> profiles is achieved by running the TM4 chemistry transport model (CTM) forward in time based on forecast ECMWF meteo and assimilated NO<sub>2</sub> information from all previously observed orbits. OMI NO<sub>2</sub> slant columns, after correction for spurious across-track variability, show a random error for individual pixels of approximately  $0.7 \times 10^{15}$  molec cm<sup>-2</sup>. Cloud parameters from OMI's O<sub>2</sub>-O<sub>2</sub> algorithm have similar frequency distributions as retrieved from SCIAMACHY's Fast Retrieval Scheme for Cloud Observables (FRESCO) for August 2006. On average, OMI cloud fractions are higher by 0.011, and OMI cloud pressures exceed FRESCO cloud pressures by 60 hPa. A sequence of OMI observations over Europe in October 2005 shows OMI's capability to track changeable NO<sub>x</sub> air pollution from day to day in cloud-free situations.

### 1 Introduction

The daily global coverage and the nadir pixel size of 24×13 km<sup>2</sup> make OMI on the Earth Observing System (EOS) Aura satellite well suited to observe the sources of air pollution with an unprecedented spatial and temporal coverage. Recently, satellite-based observations of tropospheric NO<sub>2</sub> have been proven useful in estimating anthropogenic emissions of nitrogen oxides (Leue et al., 2001; Martin et al., 2003, 2006; Beirle et al., 2003; Richter et al., 2005; van der A et al., 2006), in observing emissions by soils (Jaeglé et al., 2004), and in putting constraints on NO<sub>x</sub> production by lightning (Beirle et al., 2004, 2006; Boersma et al., 2005). Tropospheric NO<sub>2</sub> columns derived from the Global Ozone Monitoring Instrument (GOME) have been compared with outputs from various-scale models (Velders et al., 2001; Lauer et al., 2002; Savage et al., 2004; Ma et al., 2006). The results of the regional-scale chemistry-transport model CHIMERE have been evaluated against GOME and SCIAMACHY-derived tropospheric NO<sub>2</sub> columns (Konovalov et al., 2004; Blond et al., 2007). These comparisons have clearly demonstrated the potential of satellite NO<sub>2</sub> data sets for model evaluation and emission estimates.

On the other hand, sometimes large and systematic differences persist between retrievals by different groups (van Noije et al., 2006), calling into question the quality of space-based constraints on NO<sub>x</sub> sources. But validation efforts for various retrievals show acceptable accuracy (Heland et al., 2002; Petritoli et al., 2004; Martin et al., 2004, 2006; Petritoli et al., 2005; Cede et al., 2006; Ordóñez et al., 2006; Schaub et al., 2006) for GOME and SCIAMACHY NO<sub>2</sub>.

The unique characteristics of OMI – the small pixel size and daily global coverage – allow for an important contribution to air quality monitoring and modelling. GOME has a resolution of 320×40 km<sup>2</sup>, too coarse to resolve the areas with high emissions that are relevant in regional air quality modelling, e.g. medium-sized cities. SCIAMACHY's

Correspondence to: K. F. Boersma  
(boersma@fas.harvard.edu)

horizontal resolution is 60×30 km<sup>2</sup> but it needs six days to achieve global coverage. Despite the fact that interesting regional-scale daily variability has been observed with SCIAMACHY (Blond et al., 2007), it is not well suited for a day-to-day monitoring of air quality. The daily coverage of OMI has been an important motivation to set up the near-real time NO<sub>2</sub> retrieval system described in this paper.

An additional motivation originates from the data set of tropospheric NO<sub>2</sub> columns retrieved from the GOME and SCIAMACHY instruments that now spans more than 10 years (1996–2007) and is publicly available through (<http://www.temis.nl>). NO<sub>2</sub> data sets from GOME and SCIAMACHY have been retrieved with one and the same retrieval-assimilation-modelling approach described in Boersma et al. (2004) and show excellent mutual consistency (van der A et al., 2006). The OMI NO<sub>2</sub>-retrievals described here are expected to add considerable value to the GOME and SCIAMACHY dataset.

Health regulations concerning air quality require a routine monitoring, typically on an hourly basis, of surface concentrations of several species including NO<sub>2</sub>. Clearly, this requirement cannot be directly fulfilled by satellite instruments in general, nor by OMI in particular. Nevertheless we anticipate that instruments like OMI will make essential contributions to air quality monitoring and modelling:

- Daily maps of NO<sub>2</sub> columns by OMI (<http://www.temis.nl>) show extensive transport features that are changing from day to day, and that are politically interesting as they directly show air pollution being transported across national borders. These changeable distributions can be directly compared with model output, and they constitute strong tests for the description of horizontal and vertical transport processes, as well as NO<sub>x</sub> removal processes.
- A direct relationship exists between columns of NO<sub>2</sub> and surface emissions of NO<sub>x</sub>. OMI data can thus be combined with regional-scale models through inverse modeling or data assimilation to adjust or improve emission estimates in the model and to detect unknown sources.
- Incidental releases, such as from major fires, can be monitored and quantified, and subsequent plumes can be tracked from day to day.
- A routine assimilation of satellite data may improve air quality “nowcasting” and forecasting capabilities, and may thereby contribute to the monitoring of emission and health regulations.

All these applications are new and largely untested. Despite this, there exists a considerable interest in the community to establish atmospheric chemistry data assimilation systems that will exploit the available satellite data sets of atmospheric composition and air pollution. One example is the

European GEMS project (Global and regional Earth-system (Atmosphere) Monitoring using Satellite and in-situ data; (<http://www.ecmwf.int/research/EU/projects/GEMS/>)) which is scheduled to deliver an operational atmospheric composition assimilation system by 2009.

This paper presents a new retrieval algorithm designed for near-real time retrieval of tropospheric NO<sub>2</sub> from OMI. This algorithm differs from the standard, off-line OMI NO<sub>2</sub> retrieval-procedure that is a joint NASA/KNMI effort (Bucsela et al., 2006). These differences are discussed in Sect. 3.1. In Sect. 2 we discuss OMI characteristics and the fast data transport from the satellite to the retrieval computer system. The retrieval is discussed in Sect. 3, with a focus on the innovations with respect to previous NO<sub>2</sub> column retrieval work at KNMI. Section 4 is devoted to errors in the NO<sub>2</sub> slant columns. The stratospheric correction and computation of the air mass factor (AMF) are described in Sect. 5. As SCIAMACHY and OMI cloud retrieval use different spectral features, we also discuss in Sect. 5 the consistency of the OMI O<sub>2</sub>–O<sub>2</sub> cloud product with the SCIAMACHY FRESCO cloud retrievals. In Sect. 6 we show some examples of OMI’s capabilities, followed by conclusions in Sect. 7.

## 2 OMI overview

### 2.1 Ozone Monitoring Instrument

The Dutch-Finnish Ozone Monitoring Instrument (OMI) on NASA’s EOS Aura satellite is a nadir-viewing imaging spectrograph measuring direct and atmosphere-backscattered sunlight in the ultraviolet-visible (UV-VIS) range from 270 nm to 500 nm (Levelt et al., 2006a). EOS Aura was launched on 15 July 2004 and traces a Sun-synchronous, polar orbit at approximately 705 km altitude with a period of 100 min and a local equator crossing time between 13:40 and 13:50 local time. In contrast to its predecessors GOME and SCIAMACHY, instruments operating with scanning mirrors and one-dimensional photo diode array detectors, OMI has been equipped with two two-dimensional CCD detectors. The CCDs record the complete 270–500 nm spectrum in one direction, and observe the Earth’s atmosphere with a 114° field of view, distributed over 60 discrete viewing angles, perpendicular to the flight direction. OMI’s wide field of view corresponds to a 2600 km wide spatial swath on the Earth’s surface for one orbit, large enough to achieve complete global coverage in one day. The exposure time of the CCD-camera measures 2 s, corresponding to a spatial sampling of 13 km along track (2 s×6.5 km/s, the latter being the orbital velocity projected onto the Earth’s surface). Across track the size of an OMI pixel varies with viewing zenith angle from 24 km in the nadir to approximately 128 km for the extreme viewing angles of 57° at the edges of the swath.

OMI has three spectral channels; UV1 (270–310 nm) and UV2 (310–365 nm) are covered by CCD1. CCD2 covers the VIS-channel from 365–500 nm with a spectral sampling of 0.21 nm and a spectral resolution of 0.63 nm. It is in this channel that the spectral features of NO<sub>2</sub> are most prominent. The spectral sampling rate (resolution/sampling) is  $\sim 3$ , large enough to avoid spectral undersampling or aliasing difficulties in the spectral fitting process. A polarization scrambler makes the instrument insensitive to the polarization state of the reflected Earth radiance to less than 0.5%.

During nominal operations OMI takes one measurement of the solar irradiance per day. Radiometric calibration is accomplished in-flight by a series of special on-board measurements that involve monitoring detector degradation with a white-light source, and dark signal measurements when OMI is at the dark side of the Earth. Spectral calibration is achieved by a cross-correlation of Fraunhofer lines in theoretical and observed in-flight irradiance spectra. For more details on the instrument and calibration procedures, the reader is referred to Dobber et al. (2005, 2006).

Retrievals of ozone column and vertical distribution (as well as BrO and OCIO columns) are meant to address the first EOS Aura science question whether the ozone layer is recovering. Of no less importance are the retrievals of trace gases related to air pollution and the production of photochemical smog, i.e. NO<sub>2</sub>, HCHO (Kurosu et al., 2005), and SO<sub>2</sub> (Krotkov et al., 2006). In addition, cloud and aerosol parameters, and UV-B surface flux are derived from OMI. For an overview of EOS-AURA and OMI targets, see Levelt et al. (2006b).

## 2.2 Data transport

Unprocessed OMI science data are down-linked once per orbit (100 min) to one of the Ground Stations (Alaska, Svalbard (Spitsbergen), or Wallops (Virginia)). Subsequently the OMI data are sent to the EOS Data Operations System (EDOS) at NASA GSFC in Maryland (USA). At GSFC, processing of raw OMI data results in Rate-Buffered Data, Expedited Data, and Production Data. Near-real time processing is based on Rate-Buffered Data (RBD). RBD data are made available with the highest priority, at the expense of data integrity. The other data types are scheduled for off-line level 2 retrievals.

EDOS forwards the RBD data to the OMI Science Investigator-led Processing System (SIPS), where production starts as soon as all engineering, ancillary and science data have been received. Then, the resulting level 0 data sets (in Analog to Digital Units) are processed into level 1b data, i.e. estimated radiances and irradiances in units of W/m<sup>2</sup>/nm(/sr) (van den Oord et al., 2006). The only difference with standard production at this time is that the near-real time processing uses the predicted altitude and ephemeris data received from the spacecraft rather than definitive altitude and ephemeris data. Using predicted orbital parame-

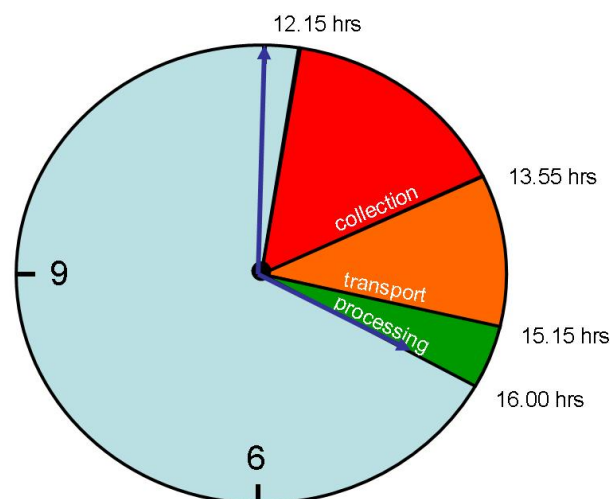


**Fig. 1.** OMI science data is linked down to ground stations once per orbit, resulting in a time delay between the OMI observations and reception at the ground station of at most 100 min. The collection, time-ordering, consecutive transfers, and level 1b and 2 processing, takes approximately 80 min. Final processing, image generation and web publishing generally occurs within 45 min.

ters may lead to errors in geolocation parameters (latitude, longitude, solar, viewing, and azimuth angles), but in practice these errors are small. Once OMI level 1b data has been generated at the SIPS, the O<sub>2</sub>–O<sub>2</sub> cloud level 1–2 algorithm (Acarreta et al., 2004) is run, followed by the DOAS ozone (Veeffkind and De Haan, 2002) and NO<sub>2</sub> slant column spectral fitting retrieval algorithms. As soon as the ozone and NO<sub>2</sub> slant column files are available, they are picked up by the OMI Dutch Processing system (ODPS) and forwarded to the processing system at KNMI developed within the DOMINO project (see acknowledgment). Subsequent steps are intrinsic parts of the near-real time retrieval algorithm and are described in the next section.

Typical data volumes per orbit are 450 MB level 0 data, 400 MB level 1b data, and 17 MB NO<sub>2</sub> slant column data (including cloud retrievals). Processed orbital data arrives at KNMI on average within three hours after the start of an orbit. An orbit takes 100 min (indicated as the red part of Fig. 1) and the process described above (downlink, transfer to EDOS, transfer to SIPS, level 1b and 2 processing, and transfer to KNMI) takes 80 min (the orange part in Fig. 1). Final processing from NO<sub>2</sub> slant columns to tropospheric vertical columns is typically faster than 2 min on a linux workstation. Including the generation of images and web publishing, the processing step takes less than 45 min (the green part of Fig. 1), so that data and images are available for the public at approximately 16:00 local time.

### 3 Algorithm description

#### 3.1 Heritage: the retrieval-assimilation-modelling approach

The near-real time NO<sub>2</sub> retrieval algorithm (DOMINO version: TM4NO2A-OMI v0.8, February 2006) is based on the retrieval-assimilation-modelling approach (hereafter: RAM) described in Boersma et al. (2004). The RAM-approach has been applied at KNMI to generate a tropospheric NO<sub>2</sub> data base from GOME and SCIAMACHY measurements. The RAM approach consists of a three-step procedure:

1. a slant column density is determined from a spectral fit to the Earth reflectance spectrum with the so-called DOAS approach (differential absorption spectroscopy, e.g. Platt, 1994; Boersma et al., 2002; Bucselá et al., 2006),
2. the stratospheric contribution to the slant column is estimated from assimilating slant columns into a CTM including stratospheric chemistry and wind fields, and
3. the residual tropospheric slant column is converted into a vertical column by application of a tropospheric air mass factor (AMF).

The standard, off-line NO<sub>2</sub> product (Bucselá et al., 2006) and the near-real time retrieval have step 1 in common. This step is discussed in detail in Sect. 3.2 and 3.3. Step 2 and 3 are (partly) different between the OMI off-line and NRT algorithms. Table 1 summarizes similarities and differences between the two retrievals.

A NO<sub>2</sub> data set (from April 1996 onwards) has been generated with the RAM-approach from GOME and SCIAMACHY. The set contains tropospheric NO<sub>2</sub> columns along with error estimates and averaging kernels (Eskes and Boersma, 2003) for every individual pixel and is publicly available through <http://www.temis.nl>. Schaub et al. (2006) showed that RAM-GOME tropospheric NO<sub>2</sub> over Northern Switzerland in the period 1996–2003 compares favourably to NO<sub>2</sub> profiles observed with in-situ techniques. Blond et al. (2007) reported considerable consistency between RAM-SCIAMACHY tropospheric NO<sub>2</sub> columns and both surface observations as well as simulations from the regional air-quality model CHIMERE over Europe, especially over moderately polluted rural areas. Merged GOME and SCIAMACHY observations showed a distinct increase in NO<sub>2</sub> columns from 1996 to 2003 over China, consistent with a strong growth of NO<sub>x</sub> emissions in that area (van der A et al., 2006). Moreover, this paper showed an almost seamless continuity from GOME to SCIAMACHY NO<sub>2</sub> values retrieved with the same RAM-approach. This finding provides confidence in the consistency of the two data sets and their retrieval method, even though they originated from two different instruments (with similar overpass times of 10:30 (GOME) and 10:00 local time (SCIAMACHY)).

Tropospheric NO<sub>2</sub> columns are retrieved as follows:

$$V_{tr} = \frac{S - S_{st}}{M_{tr}(\mathbf{x}_{a,tr}, \mathbf{b})}, \quad (1)$$

with  $S$  the slant column density from step 1,  $S_{st}$  the stratospheric slant column obtained from step 2, and  $M_{tr}$  the tropospheric AMF that depends on the a priori NO<sub>2</sub> profile  $\mathbf{x}_{a,tr}$  and the set of forward model parameters  $\mathbf{b}$  including cloud fraction, cloud pressure, surface albedo, and viewing geometry. The vertical sensitivity of OMI NO<sub>2</sub> strongly depends on surface albedo and the presence of clouds (Eskes and Boersma, 2003).

For the RAM-approach and the NRT-retrieval, AMFs and averaging kernels are computed with a pseudo-spherical version of the DAK radiative transfer model (Stammes, 2001) as described in Boersma et al. (2004). Given the best estimate of the forward model parameters the DAK forward model simulates the scattering and absorbing processes that define the average optical path of photons from the Sun through the atmosphere to the OMI.

Also similar as in our RAM-approach for off-line retrievals, we obtain here the a priori NO<sub>2</sub> profile shapes ( $\mathbf{x}_{a,tr}$ ) from the global chemistry-transport model TM4 at a resolution of 2° latitude by 3° longitude and 35 vertical levels extending up to 0.38 hPa. Given the few available in situ NO<sub>2</sub> measurements, a global 3-D model of tropospheric chemistry is the best source of information for the vertical distribution of NO<sub>2</sub> at the time and location of the OMI measurement. The TM4 model is driven by forecast and analysed six hourly meteorological fields from the European Centre for Medium Range Weather Forecast (ECMWF) operational data. These fields include global distributions for horizontal wind, surface pressure, temperature, humidity, liquid and ice water content, cloud cover and precipitation. A mass conserving preprocessing of the meteorological input is applied according to Bregman et al. (2003). Key processes included are mass conserved tracer advection, convective tracer transport, boundary layer diffusion, photolysis, dry and wet deposition as well as tropospheric chemistry including non-methane hydrocarbons to account for chemical loss by reaction with OH (Houweling et al., 1998). In TM4, anthropogenic and natural emissions of NO<sub>x</sub> are based on results from the EU POET-project (Precursors of Ozone and their Effects on the Troposphere) for the year 1997 (Olivier et al., 2003). Including free tropospheric emissions from air traffic (0.8 Tg N/yr) and lightning (5 Tg N/yr), total NO<sub>x</sub> emissions for 1997 amount to 46 Tg N/yr.

Because OMI does not detect the O<sub>2</sub> A band at 760 nm, we use cloud parameters retrieved from the VIS-channel using the O<sub>2</sub>–O<sub>2</sub> absorption feature at 477 nm (Acarreta et al., 2004). The cloud retrieval is based on the same set of assumptions (i.e. clouds are modelled as Lambertian reflectors with albedo 0.8) as the FRESKO-algorithm (Koelemeijer et al., 2001). Before launch, the precision of the O<sub>2</sub>–O<sub>2</sub> cloud fraction and cloud pressure was discussed in Acarreta

**Table 1.** Overview of the two OMI tropospheric NO<sub>2</sub> retrievals.

|                                     | OMI standard product (Bucsela et al., 2006)                           | OMI near-real time (this work)                              |
|-------------------------------------|---|---|
| Slant column                        | DOAS (405–465 nm)   | DOAS (405–465 nm)   |
| Across-track variability correction | Correction factors based on 24-h data <sup>1</sup>                    | Correction factors computed per-orbit <sup>2</sup>          |
| Stratospheric slant column          | Wave-2 fitting along zonal band                                       | Data assimilation in TM4                                    |
| AMF - cloud parameters              | O <sub>2</sub> –O <sub>2</sub> (Acarreta et al., 2004)                | O <sub>2</sub> –O <sub>2</sub> (Acarreta et al., 2004)      |
| AMF - surface albedo                | GOME(Koelemeijer et al., 2003)  | TOMS/GOME <sup>3</sup>                                      |
| AMF - profile shape                 | Yearly average profile shapes from GEOS-Chem (2.5° × 2°) <sup>4</sup> | Collocated daily output at overpass time from TM4 (3° × 2°) |
| AMF - ghost column                  | Not included  | Implicit in AMF definition                                  |

<sup>1</sup> In the standard product, mean slant columns are adjusted for a given cross-track position to the mean value at all positions. The mean slant column and the mean initial AMF for each cross-track position are computed from 24-h of data using measurements obtained at latitudes between ±55°. These are used to generate a set of 60 correction constants, one for each cross-track position, which are subtracted from the slant column values before computation of the vertical columns.

<sup>2</sup> The correction for the near-real time retrieval is described in Sect. 4.1.

<sup>3</sup> Surface albedo fields are taken from a combination of Herman and Celarier (1997) and Koelemeijer et al. (2003) as described in Boersma et al. (2004).

<sup>4</sup> AMFs are corrected based on average a priori profile shapes when the retrieved slant column is larger than the estimated stratospheric slant column (Bucsela et al., 2006).

et al. (2004) with encouraging results. In Sect. 5.2.1 we test the accuracy of the O<sub>2</sub>–O<sub>2</sub> cloud parameters by comparing them to FRESCO cloud parameters retrieved by SCIAMACHY on the same days and same locations.

As for GOME and SCIAMACHY retrievals, we use a surface albedo database derived from TOMS and GOME Lambert-equivalent reflectivity (LER) measurements at 380 nm and 440 nm as described in Boersma et al. (2004). These monthly average surface albedo maps have a spatial resolution of 1° × 1.25° and represent climatological (monthly) mean situations. The uncertainty in the surface albedo is estimated to be approximately 0.01 (Koelemeijer et al., 2003; Boersma et al., 2004).

In summary, the near-real time algorithm is based on the RAM-approach used for GOME and SCIAMACHY retrievals at KNMI. The main differences with RAM are: (1) near-real time requirement, (2) different spectral fitting method, and (3) cloud inputs derived from (similar but) different algorithms.

### 3.2 Near-real time retrieval

In the RAM-approach, the estimated stratospheric NO<sub>2</sub> column (step 2) and the modelled profile shape (required for step 3), are provided by off-line assimilation and modelling based on analysed ECMWF meteorological data. In contrast, for the NRT-retrieval, the assimilation and modelling steps are operational, based on daily ECMWF meteorological analyses and forecasts.

The NRT-retrieval consists of two distinct subsystems.

The first is the TM forecast subsystem shown in Fig. 2. This forecast system is run once per day, as soon as meteorological data becomes available. The second subsystem is activated each and every time that new OMI data becomes available, and incorporates the model information provided by subsystem 1.

In the forecast subsystem (1), the actual chemical state of the atmosphere is based on the analysis and forecast run starting from the analysis of the previous day. The update consists of running the chemistry-transport model forward in time with the forecast ECMWF meteorological data and the assimilation of all available OMI NO<sub>2</sub> slant columns measurements. The updated analysis, the new actual state, is then stored as input for a subsequent time step. The outputs are the necessary inputs to the near-real time subsystem (2); the stratospheric NO<sub>2</sub> column and the NO<sub>2</sub> and temperature profiles (needed in AMF computations).

The NRT-subsystem is illustrated in Fig. 3. As soon as an orbit of observed NO<sub>2</sub> slant columns arrives at KNMI, the forecast TM stratospheric slant column, is ready and is subtracted. Subsequently, the residual tropospheric slant column is converted into a vertical column by the tropospheric AMF. The AMF is computed as described as in 3.1. The averaging kernel is also calculated for output and furthermore serves as the observation operator required in the assimilation part of the TM forecast subsystem.

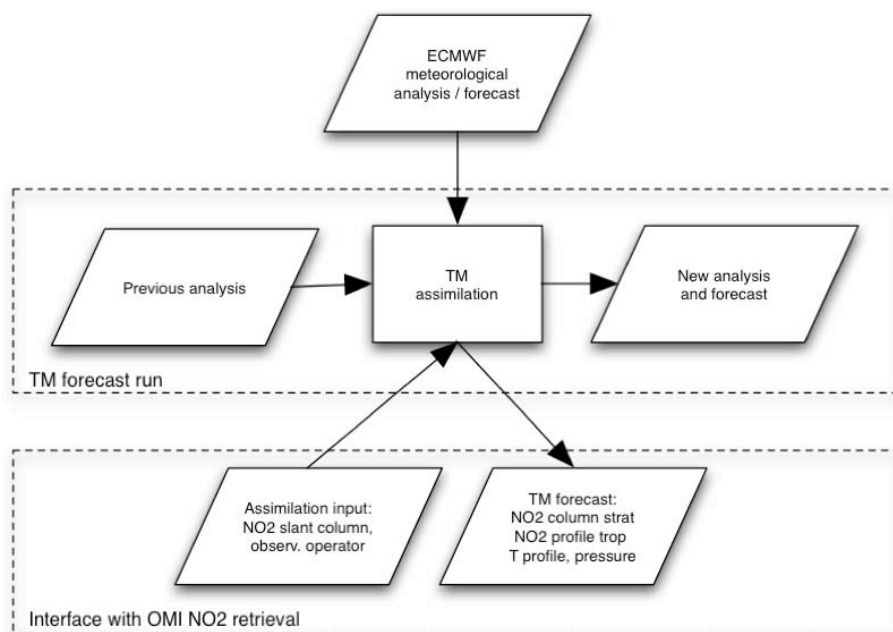


**Fig. 2.** Flowchart for the DOMINO forecast/assimilation subsystem. The lowest part shows the input-output interface with the NRT-subsystem.

### 3.3 Slant column retrieval

A second difference between the OMI near-real time and RAM off-line implementations is the wide spectral window that is used in the DOAS retrieval. For GOME and SCIAMACHY, it has been conventional wisdom that a 425–450 nm window yields the most precise and stable fitting results. For OMI a much wider fit window, 405–465 nm, has been proposed by Boersma et al. (2002) in order to compensate for OMI's lower signal-to-noise ratio (approximately 1400 under normal mid-latitude conditions) compared to GOME and SCIAMACHY (approximately 2000, Bovensmann et al., 1999) in this wavelength region. Pre-flight testing showed that a least squares fitting of reference spectra from NO<sub>2</sub>, O<sub>3</sub>, a theoretical Ring function, and a 3rd order polynomial to the reflectance spectrum yields results that are stable for multiple viewing geometries with a better than 10% NO<sub>2</sub> slant column precision (Boersma et al., 2002). Including H<sub>2</sub>O and O<sub>2</sub>–O<sub>2</sub> did not affect the fitted slant columns. The NO<sub>2</sub> absorption cross section spectrum is taken from Vandaele et al. (1998), who tabulated the cross section at different temperatures. To account for the temperature sensitivity of the NO<sub>2</sub> cross section spectrum an effective atmospheric temperature is calculated for the NO<sub>2</sub> along the average photon path. Subsequently an a posteriori correction for the difference between the computed effective temperature and the 220 K cross section spectrum used in the fitting procedure is applied (Boersma et al., 2002). The ozone absorption cross section spectrum is taken from WMO

(1975) and the theoretical Ring spectrum from De Haan (private communication, 2006) based on irradiance data by Voors et al. (2006). All reference spectra have been convolved with the OMI instrument transfer function (Dobber et al., 2005). OMI NO<sub>2</sub> slant column retrieval with synthetic and flight model data (Dobber et al., 2005) yields results that fulfill the OMI science requirement of better than 10% slant column precision (Boersma et al., 2002; Bucsele et al., 2006). However, upon first inspection of actual flight-data, systematic enhancements in the OMI NO<sub>2</sub> slant columns show up at specific satellite viewing angles. This has also been reported by Kurosu et al. (2005) for HCHO-retrievals.

## 4 Slant column density errors

### 4.1 Across-track variability

Calibration errors in the level 1b OMI irradiance measurements used here are likely responsible for across-track variability observed in the NO<sub>2</sub> slant columns. This variability will likely be significantly reduced in future level 1b releases with improved calibration data (expected in Spring 2007), using daily dark current corrections. Across-track variability appears as constant offsets for specific satellite viewing angles along an orbit, allowing for an a posteriori correction:

1. Determine the orbital segment (50 along track by 60 across track pixels in size) with the minimum variance in NO<sub>2</sub> columns.

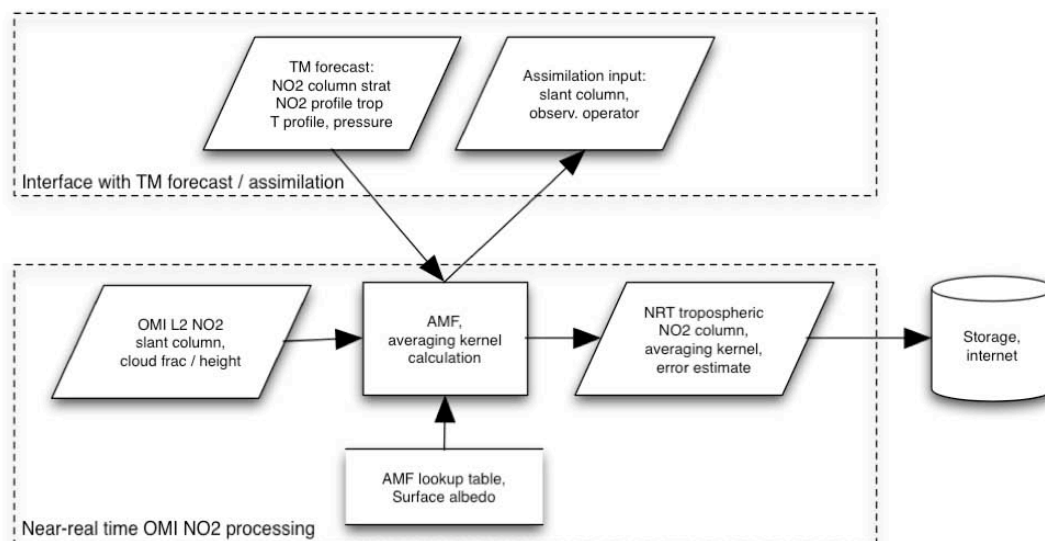


**Fig. 3.** Flowchart for the DOMINO NRT-subsystem. The upper part shows the input-output interface with the forecast/assimilation-subsystem (the lower part of Fig. 2).

2. Within this window, average the 50 NO<sub>2</sub> columns with the same viewing angle. This gives 60 average across-track NO<sub>2</sub> columns.
3. Separate low and high frequencies of the across-track columns with a Fourier analysis.
4. Perform the correction by subtracting the (high-frequency) across-track variability for all across-track rows along the orbit.

In this scheme, the selection of the minimum variance window avoids areas with large anthropogenic emissions. The high-frequencies are then interpreted as the across-track variability due to calibration errors in the OMI level 1b data. Similarly, the low frequencies describe any (weak, stratospheric) natural variability. The low frequencies are described by the first three Fourier terms. Subsequently we subtract the high-frequency signal obtained for the minimum variance window for all rows along the orbit. If it turns out to be not possible to determine a correction for a particular orbit, the across-track variability correction from the previous orbit is taken. Figure 4 shows corrections for across-track variability computed from 10 consecutive orbits measured on the same day (22 September 2004). Although the corrections have been computed from independent data, they are similar. This justifies taking the correction determined from the previous orbit if it cannot be determined from the actual orbit. Furthermore, Fig. 4 provides evidence that irradiance data are most likely at the basis of the across-track variability. All orbits shown have been retrieved with the same irradiance measurement. However, when the correction was plotted for

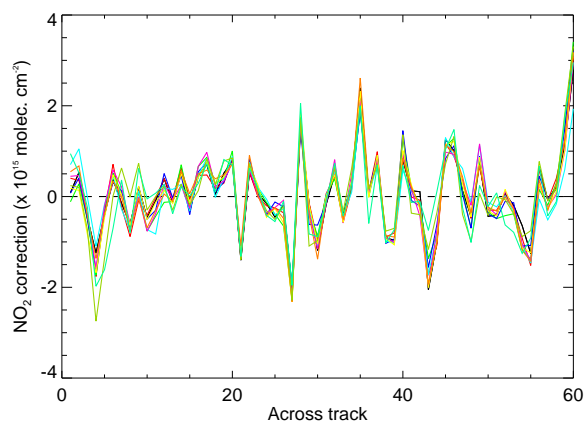


**Fig. 4.** Across-track variability corrections, computed with the method described in Sect. 4.1, for 10 consecutive orbits on 22 September 2004. Every orbital correction is shown with a unique colour.

the first orbit retrieved with a new irradiance measurement, a distinctly different correction pattern was seen (not shown).

#### 4.2 Slant column precision

We present here a statistical analysis of OMI NO<sub>2</sub> columns observed over separate 2° × 2° boxes in the meridional band between 178° and 180° W. The basic assumption is that the OMI pixels within a 2° × 2° box observe the same total vertical column over this clean part of the Pacific Ocean. Any variability in the observed total vertical columns is assumed

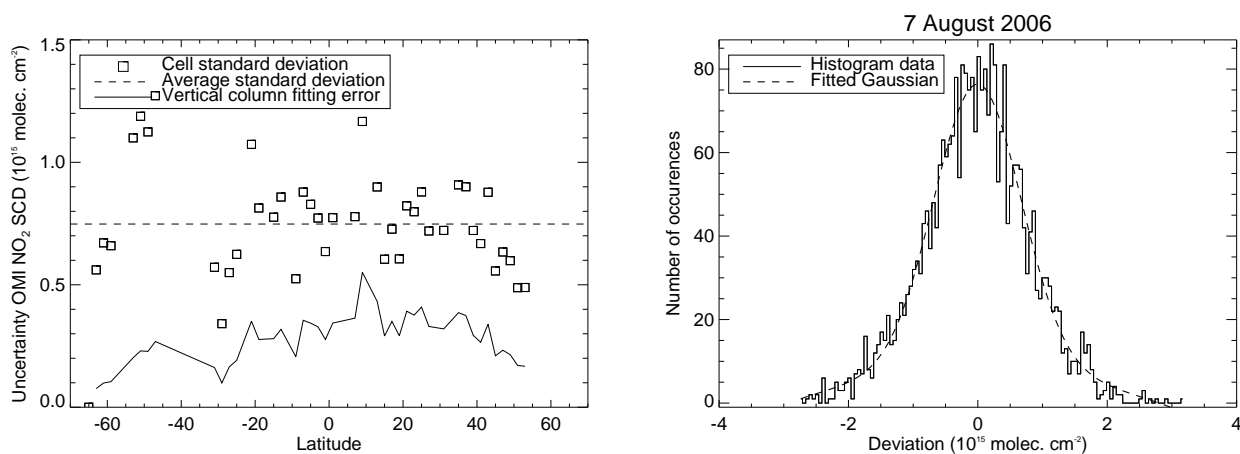


**Fig. 5.** Left panel: standard deviation of slant columns within a  $2^\circ \times 2^\circ$  (longitudes between  $178^\circ$  and  $180^\circ$  W) box as a function of latitude. The dashed line shows the meridional average of the standard deviations for all the boxes. The solid line shows the contribution of the (slant column) fitting error to the vertical column error  $M$  (i.e.  $\sigma_S/M$ ). Right panel: distribution of member deviations from box means for 2893 pixels. The dashed line shows a Gaussian function fitted to the histogram data. The width of the Gaussian corresponds to a slant column error of  $0.67 \times 10^{15}$  molec cm<sup>-2</sup>.

to originate from errors in the slant columns if the ensemble of AMFs within a box has little variability. Boxes with appreciable AMF variability have been rejected if the box-mean vertical column computed by averaging the ensemble of individual slant columns ratioed by a box-mean AMF ( $\bar{V}'$ ) differed by more than 0.1% from the box-mean vertical column computed by averaging the ensemble of individual slant columns ratioed by the original AMFs ( $\bar{V}$ ). We find that for most of the  $2^\circ \times 2^\circ$  boxes between  $60^\circ$  N and  $60^\circ$  S,  $\bar{V}$  and  $\bar{V}'$  do not differ by more than 0.1%, and thus the slant columns have been observed under almost identical viewing geometries. For these boxes, we take the standard deviation of the ensemble of slant-column as the estimate for the precision of the slant columns.

For 7 August 2006, we computed estimates for the slant column errors for every box between  $60^\circ$  S and  $60^\circ$  N. The results are shown in Fig. 5 (left panel) for boxes with a relative difference between  $\bar{V}$  and  $\bar{V}'$  of less than 0.1%. The figure shows that there is no appreciable change of fitting error with latitude. Averaged over all latitudes, the fitting error is close to  $0.75 \times 10^{15}$  molec cm<sup>-2</sup> (dashed line). For the vertical column error, the contribution from the fitting error is smaller than  $0.4 \times 10^{15}$  molec cm<sup>-2</sup> (solid line, computed as  $\sigma_S/M$ ). Figure 5 (right panel) shows the distribution of all member deviations from box means in a histogram ( $n=2893$ ). The distribution closely follows a Gaussian shape that is fitted to the histogram data. The fact that the distribution follows a Gaussian distribution is consistent with our assumption that the variability within each box is dominated by random errors in the slant columns, originating from measurement noise and possible residuals of the correction procedure. The corresponding width of the Gaussian for this

day is  $0.67 \times 10^{15}$  molec cm<sup>-2</sup>, and we interpret this as our estimate for the average slant column error of all 2893 pixels we investigated on 7 August 2006. The slant column error is the combined error from fitting noise and from any residual across-track variability. We also looked into a few other days and other longitude bands with different across-track variability corrections, and found very similar numbers.

The slant column error for an individual OMI pixel is somewhat larger than the better-than-10% ( $\approx 0.3 \times 10^{15}$  molec cm<sup>-2</sup>) number quoted in Boersma et al. (2002). This number was computed from synthetic spectra (i.e. without across-track variability) under the assumption that 4 OMI pixels would be binned (increasing signal-to-noise by a factor of 2). For individual pixels, the OMI fitting error is larger than the  $0.45 \times 10^{15}$  molec cm<sup>-2</sup> found for GOME (Boersma et al., 2004) and SCIAMACHY (I. DeSmedt, private communication), consistent with the higher signal-to-noise ratios for individual GOME and SCIAMACHY pixels than for OMI pixels.

## 5 Stratospheric contribution and tropospheric air mass factor

### 5.1 Stratospheric slant column

The stratospheric component of the NO<sub>2</sub> slant column is estimated by data-assimilation of OMI slant columns in TM4:

- Modelled NO<sub>2</sub> profiles are convolved with the appropriate averaging kernel to give model-predicted slant column densities. We take model fields that are closest in time to the mean OMI orbit time (model information is stored in UT with 30 min increments, 48 fields per day).

This limits differences between observation and model times in the assimilation to at most 55 min ( $\pm 25$  from actual vs. mean orbit time,  $\pm 30$  from model vs. mean orbit time). Taking model fields closest in time is relevant only at high latitudes where local time differences across an OMI swath are considerable and could lead to large assimilation errors if the model was just sampled at 13:30 local time. Rejecting retrievals with solar zenith angles  $> 80^\circ$ , we avoid regions with day-night transitions. The differences between observed and modelled columns (the model innovations) are used to force the modelled columns to generate an analysed state that is based on the modelled NO<sub>2</sub> distribution and the OMI observations.

- The forcing depends on weights (from observation representativeness and model errors) attributed to model and observation columns. The observation error is set to A times the modelled tropospheric slant column plus B times the modelled (assimilated) stratospheric slant column. A and B are relative errors, and are chosen as A=4 and B=0.25. This implies that the observation error rapidly increases for modelled tropospheric vertical columns larger than or of the order of  $0.5 \times 10^{15}$  molec cm<sup>-2</sup>. As a consequence, moderately and highly polluted regions obtain a small weight in the assimilation. The ratio A/B roughly reflects the high uncertainties in the tropospheric retrieval as compared to the stratosphere.
- The forcing equation (based on the Kalman filter technique) is solved with the statistical interpolation method. This involves a covariance matrix that describes the forecast error and spatial correlations. The most important characteristics of this forecast covariance matrix are: (1) the conservation of modelled profile shapes. The altitude dependence of the forecast error is set to be proportional to the local NO<sub>2</sub> profile shape. (2) The horizontal correlation model function is assumed to follow a Gaussian shape with an 1/e correlation length of 600 km. This length was derived from the assimilation of ozone in the stratosphere (Eskes et al., 2003) and should be a reasonable guess for stratospheric NO<sub>2</sub> as well. (3) In addition we introduce a correlation scaling to reduce the correlation with increasing differences in concentration (Riishøjgaard, 1998). This avoids problems with negative concentrations near sharp gradients that occur for instance at the polar vortex edge. (4) The vertical distribution of the assimilation increments is determined by the covariance matrix and the averaging kernel profile. The kernel peaks in most cases in the stratosphere, which is an additional reason why the adjustment caused by the assimilation is mainly taking place in the stratosphere.

- The adjustments made by the assimilation are therefore mainly occurring in the stratosphere at places where the tropospheric concentrations are low. The stratospheric information inserted by the assimilation is transported to the stratosphere above more polluted areas by the advection in the model.
- The model NO<sub>x</sub> species (NO, NO<sub>2</sub>, NO<sub>3</sub>, N<sub>2</sub>O<sub>5</sub>, HNO<sub>4</sub>) are assumed to be fully correlated and are all scaled in the same way as NO<sub>2</sub>.
- Based on the most recent analysed state, a forecast run of the model predicts the stratospheric field. This is used by the near-real time retrieval branch as shown in Fig. 2.

For further reading on the assimilation method we refer to Eskes et al. (2003). The advantage of the approach is that slant column variations due to stratospheric dynamics are now accounted for in the retrieval. The purpose is to improve the detection limit for tropospheric NO<sub>2</sub> columns. An additional advantage is that the assimilation scheme provides a statistical estimate of the uncertainty in the stratospheric slant column. Generally, this uncertainty is on the order of  $0.1\text{--}0.2 \times 10^{15}$  molec cm<sup>-2</sup>, much smaller than the slant column uncertainty. Hence, the detection limit in our method is mainly determined by the random slant column error ( $\sigma_S$ ) that is easily averaged out by taking large numbers of observations. Not accounting for stratospheric dynamics however, would lead to systematic errors in the estimate of the stratospheric column (Boersma et al., 2004) that cannot easily be averaged out and would raise the detection threshold.

## 5.2 Tropospheric air mass factor

We convert the tropospheric slant column into a vertical column by using a tropospheric AMF (Eq. 1). For OMI NRT we follow as much as possible the same approach (same look-up tables, computational methods) as for the GOME and SCIAMACHY data set described in Sect. 3.1. But the forward model input parameters cloud fraction and cloud pressure differ between the OMI NRT and the GOME and SCIAMACHY RAM retrievals. This, along with the much finer spatial resolution of OMI compared to GOME, is expected to lead to different error budgets for OMI tropospheric NO<sub>2</sub> than for GOME and SCIAMACHY.

### 5.2.1 Cloud parameters

DOAS-type retrievals are very sensitive to errors in cloud parameters. Boersma et al. (2004) showed that errors in FRESCO cloud fractions of  $\pm 0.05$  lead to retrieval errors of up to 30% for situations with strong NO<sub>2</sub> pollution. Errors in the cloud pressure may also affect retrievals, especially in situations where the retrieved cloud top is located within a polluted layer. In such situations, errors in the cloud pressure of 50 hPa lead to retrieval errors of up to 25%.

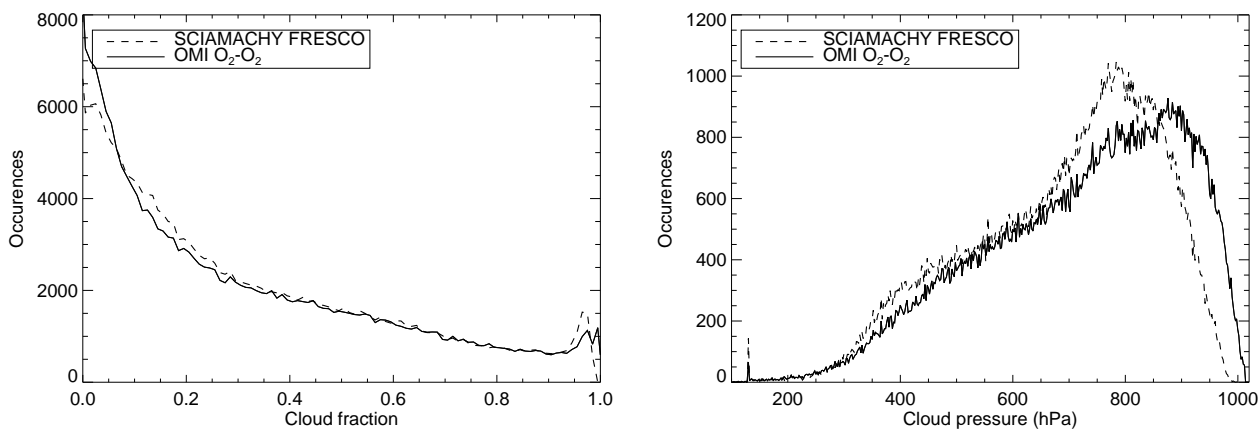


**Fig. 6.** Left panel: histogram of  $0.5 \times 0.5 \times$  gridded effective cloud fractions from SCIAMACHY FRESKO (dashed line) and OMI O<sub>2</sub>–O<sub>2</sub> for seven consecutive days (5–11 August 2006). Right panel: histogram of  $0.5 \times 0.5 \times$  gridded effective cloud pressures from SCIAMACHY FRESKO (dashed line) and OMI O<sub>2</sub>–O<sub>2</sub> for seven consecutive days (5–11 August 2006). Only observations with a cloud fraction higher or equal to 0.05 are shown.

Here we evaluate any differences between cloud parameters retrieved by SCIAMACHY and OMI. FRESKO applied on GOME measurements compared favourably to AVHRR (Koelemeijer et al., 2001) and ISCCP (Koelemeijer et al., 2002) cloud fractions (differences  $<0.02$ ) and cloud pressure (differences  $<50$ – $80$  hPa). More relevantly, Fournier et al. (2006) showed that FRESKO cloud parameters are in good agreement with other SCIAMACHY cloud algorithms, and estimate that the accuracy of the effective cloud fraction from FRESKO is better than 0.05 for all surfaces except snow and ice.

The retrieval methods for SCIAMACHY (FRESKO) and OMI (O<sub>2</sub>–O<sub>2</sub>) are based on the same principles, i.e. they both retrieve an effective cloud fraction, that holds for a cloud albedo of 0.8, and to do so, they both use the continuum top-of-atmosphere reflectance as a measure for the brightness, or cloudiness, of a scene. Furthermore they both use the depth of an oxygen band as a measure for the length of the average photon path from the Sun, through the atmosphere back to the satellite instrument. The length of this light path is converted to cloud pressure. On the other hand, there are significant differences between the cloud parameter retrievals from SCIAMACHY and OMI:

1. FRESKO uses reflectances measured inside and outside of the strong oxygen A band (758–766 nm), whereas OMI uses the weakly absorbing O<sub>2</sub>–O<sub>2</sub> band at 477 nm.
2. FRESKO and O<sub>2</sub>–O<sub>2</sub> have different sensitivities to cloud pressure. This originates from the use of absorption by a single molecule (FRESKO, O<sub>2</sub> A band), scaled with oxygen number density, versus the use of absorption by a collision complex (O<sub>2</sub>–O<sub>2</sub>), scaled with oxygen number density squared. Although this dependence

is taken into account in the retrieval algorithm, it is expected to lead to higher cloud pressures for the O<sub>2</sub>–O<sub>2</sub> cloud algorithm.

3. FRESKO does not account for Rayleigh scattering, whereas the O<sub>2</sub>–O<sub>2</sub> algorithm does. Not accounting for Rayleigh scattering leads to cloud pressures to be underestimated for small cloud fractions (Wang et al., 2006).
4. SCIAMACHY observes clouds at 10:00, and OMI at 13:45 local time.

Because SCIAMACHY and OMI observe the Earth at different times, FRESKO and O<sub>2</sub>–O<sub>2</sub> cloud parameters cannot be compared directly. However, since temporal variation in global cloud fraction and cloud pressure between 10:00 and 13:45 local time is small (Bergman and Salby, 1996), frequency distributions of cloud parameters may be compared as an evaluation of consistency between the two. Here we compare SCIAMACHY FRESKO cloud retrievals version SC-v4 (August 2006, with improved desert surface albedos) to OMI O<sub>2</sub>–O<sub>2</sub> retrievals v1.0.1.1 (available since 7 October 2005, orbit 6541). We focus on locations between 60° N and 60° S to avoid situations with ice and snow, where cloud retrieval traditionally is difficult. We gridded FRESKO and O<sub>2</sub>–O<sub>2</sub> cloud parameters to a common  $0.5^\circ \times 0.5^\circ$  grid and selected only grid cells filled with successfully retrieved cloud values for both FRESKO and O<sub>2</sub>–O<sub>2</sub>. Doing so, we obtain SCIAMACHY and OMI cloud parameter distributions on a spatial grid comparable to the SCIAMACHY grid ( $30 \times 60$  km<sup>2</sup>) that have been sampled on the same days and locations.

Figure 6 (left panel) shows the cloud fraction distribution as observed by FRESCO (dashed line) and O<sub>2</sub>–O<sub>2</sub> averaged over the period 5–11 August 2006. The distributions show a high degree of similarity, with the smallest effective cloud fractions observed most often. The differences between the two distributions are most appreciable for small effective cloud fractions, with OMI more frequently observing cloud fractions smaller than 0.05, and SCIAMACHY more frequently observing cloud fractions in the 0.05–0.20 range. These differences are likely related to different surface albedo data bases used in the cloud retrievals, and the way effective cloud fractions outside the 0.0–1.0 range are treated. The O<sub>2</sub>–O<sub>2</sub> retrieval uses the TOMS/GOME surface albedo datasets at 463 and 494.5 nm, consistent with albedos used for NO<sub>2</sub> AMF computations. But for FRESCO, the GOME albedo dataset at 760 nm is used. Since OMI's horizontal resolution is much finer than the 1°×1° surface albedo datasets, this will lead to cloud fraction errors, especially for small cloud fractions. On average for 5–11 August 2006, FRESCO observes a mean effective cloud fraction of 0.311, and O<sub>2</sub>–O<sub>2</sub> observes 0.300. The small mean difference between FRESCO and O<sub>2</sub>–O<sub>2</sub> of 0.011 is encouraging and gives a first order indication of the accuracy of the O<sub>2</sub>–O<sub>2</sub> cloud fraction retrieval.

Wang et al. (2006) showed that taking into account Rayleigh scattering in the GOME FRESCO retrieval on average increases cloud pressures by 60 hPa for cloud fractions larger than 0.1. To avoid the effects of neglecting Rayleigh scattering in our comparison of FRESCO and O<sub>2</sub>–O<sub>2</sub> (that does account for Rayleigh scattering), we focused on situations with cloud fractions higher or equal to 0.05, where the signal from Rayleigh scattering is outshined by the signal from the cloudy part of the scene. Figure 6 (right panel) shows the distributions of cloud pressures observed by FRESCO (dashed line) and O<sub>2</sub>–O<sub>2</sub> averaged over the period 5–11 August 2006. O<sub>2</sub>–O<sub>2</sub> more frequently retrieves high cloud pressures than FRESCO. On average, O<sub>2</sub>–O<sub>2</sub> cloud pressures are 58 hPa higher than FRESCO. As discussed above, O<sub>2</sub>–O<sub>2</sub> retrievals are more sensitive to levels deeper in the cloud, as the absorber slant column scales with the oxygen number density squared profile rather than with the single oxygen molecule number density profile. It is important for the NO<sub>2</sub> retrieval to use the most appropriate cloud pressure in the context of the AMF computation. The “best” cloud pressure is the level that, within the concept of the Lambertian reflector, indicates the effective scattering height for photons (in the 405–465 nm range). Dedicated validation campaigns with simultaneous observations of NO<sub>2</sub> profiles and cloud parameters that coincide with OMI observations will help address these issues.

### 5.2.2 Profile shape and representativity issues

Errors in the a priori profiles obtained from a 3-D CTM give rise to approximately 10% error in the retrieved NO<sub>2</sub>

columns (Boersma et al., 2004). Since then, Martin et al. (2004) and Schaub et al. (2006) showed that vertical distributions of NO<sub>2</sub> over the southern U.S. and over northern Switzerland calculated with a CTM (GEOS-Chem and TM4 respectively) are consistent with observed NO<sub>2</sub> profiles in these regions, increasing confidence in the model-derived a priori profile shapes.

For OMI (as well as for reprocessed GOME and SCIAMACHY data), a priori NO<sub>2</sub> profile shapes are obtained from TM4. TM4 vertical distributions are sampled at 13:30 local time at 3°×2°. This resolution is too coarse to resolve vertical distributions at OMI-scale resolution (roughly 0.1°×0.1°). Thus a certain degree of spatial smearing or smoothing may be expected. This also holds for sub-grid variation in albedo, for instance as a result of land-sea or land-snow transitions. One other source of error is surface pressure (or altitude). Retrieval algorithms that use surface pressures from a coarse-resolution CTM-run typically under-sample surface pressure over regions with marked topography. For instance over northern Switzerland this leads to significant retrieval errors (Schaub et al., 2007), suggesting that retrievals need to use surface pressure fields at a resolution compatible with the satellite observations.

### 5.2.3 Error budget

Table 2 compares contributions to AMF errors for polluted situations as presented in Boersma et al. (2004) for GOME to our best estimates for OMI in this work. We estimate that the uncertainty in the O<sub>2</sub>–O<sub>2</sub> cloud fractions is ±0.05. Although the cloud pressure uncertainty for OMI is comparable to that for GOME, there is a stronger sensitivity to cloud pressure errors for low clouds (OMI cloud pressures are on average 58 hPa higher than FRESCO cloud pressures) within the polluted NO<sub>2</sub> layer (see Fig. 5b in Boersma et al., 2004). For GOME, with pixel sizes comparable to the grid size of the forward model input parameters (albedo, profile shape, surface pressure), horizontal undersampling errors could be discarded. For OMI this can no longer be done. However, horizontal undersampling effects are relevant for some regions and times only. For instance, coarse-gridded surface pressures and albedos over a flat, rather homogeneous area like northern Germany will have little effect on fine-scale OMI retrievals. Over that same area though, spatial gradients in NO<sub>2</sub> profiles are not resolved by the 3° by 2° TM4 model, and this may lead to smearing errors. Since we have little quantitative information about undersampling errors, and because their effect is limited to certain locations and times (and highly variable), we indicate them as  $\epsilon_u$  (unknown undersampling error). Table 2 shows that the AMF error budget for individual retrievals from well quantified error sources is similar: 29% for GOME and 31% for OMI. However, horizontal undersampling errors may contribute considerably to especially OMI AMF errors for specific locations and times. Again, these issues may be addressed

**Table 2.** Overview of forward model error contributions to the (relative) tropospheric AMF ( $M_{Tr}$ ) uncertainty for GOME and OMI.  $\epsilon_{u_a}$  is the unknown error due to spatial albedo undersampling,  $\epsilon_{u_p}$  due to spatial profile shape undersampling, and  $\epsilon_U$  the overall undersampling AMF error that is highly variable in space and time.

| Error source                | GOME (Boersma et al., 2004) |                      | OMI (this work)                      |                                     |
|-----------------------------|-----------------------------|----------------------|--------------------------------------|-------------------------------------|
|                             | Uncertainty                 | Uncertainty $M_{Tr}$ | Uncertainty                          | Uncertainty $M_{Tr}$                |
| Surface albedo              | 0.02                        | 15%                  | $0.02 + \epsilon_{u_a}$ <sup>1</sup> | $15\% + \epsilon_{u_a}$             |
| Cloud fraction <sup>2</sup> | 0.05                        | 30%                  | 0.05                                 | 30%                                 |
| Cloud pressure              | 50–80 hPa                   | 2% <sup>3</sup>      | 60 hPa                               | 15% <sup>4</sup>                    |
| Profile shape               | N.A.                        | 9%                   | N.A.                                 | $9\% + \epsilon_{u_p}$ <sup>5</sup> |
| Total AMF error             |                             | 29%                  |                                      | $31\% + \epsilon_U$                 |

<sup>1</sup> $\epsilon_{u_a}$  represents the unknown horizontal albedo undersampling error related to the horizontal resolution of OMI pixels ( $0.15^\circ \times 0.15^\circ$ ) relative to the surface albedo database ( $1^\circ \times 1.25^\circ$ ).

<sup>2</sup>Retrieved cloud fractions may be affected by aerosols, contributing to the uncertainty in the AMF.

<sup>3</sup>Estimate based on observed cloud pressures from GOME that are generally above the planetary boundary layer as described in Boersma et al. (2004).

<sup>4</sup>OMI cloud pressures are more likely situated in the planetary boundary layer than GOME cloud pressures. Sensitivity to cloud pressure errors is largest for clouds within the boundary layer (Fig. 5b in Boersma et al. (2004)).

<sup>5</sup> $\epsilon_{u_p}$  represents the unknown horizontal profile undersampling error related to the horizontal resolution of OMI pixels ( $0.15^\circ \times 0.15^\circ$ ) relative to the TM4 grid cells ( $3^\circ \times 2^\circ$ ).

through dedicated validation efforts and retrieval improvements including the use of high(er)-resolution surface pressure and albedo data bases, and improved spatial resolution chemistry-transport models.

Table 3 summarizes the contribution of various errors to the overall error budget for individual retrievals in cloud-free situations. Pixels are defined as cloud-free when the cloud radiance fraction does not exceed 50%, which corresponds to effective cloud fractions smaller than 15–20%. For comparison, in Table 3 we also included error estimates for RAM-GOME retrievals. We do not explicitly correct for aerosols as these influence cloud retrievals. Modified cloud parameters indirectly account for the effect of aerosols on the retrieval (Boersma et al., 2004). The uncertainty in the AMF is determined by errors in the forward model parameters as shown in Table 2. We estimate that a rough 1-sigma uncertainty for an individual OMI retrieval can be expressed as a base component (from spectral fitting uncertainty divided by AMF value, see Eq. 5 in Boersma et al., 2004) plus a relative uncertainty in the 10%–40% range due to AMF uncertainty. The base component is in the  $0.5\text{--}1.5 \times 10^{15}$  molec cm<sup>-2</sup> range ( $0.5 \times 10^{15}$  molec cm<sup>-2</sup> for situations with high (tropospheric) AMF values,  $1.5 \times 10^{15}$  molec cm<sup>-2</sup> for situations with low tropospheric AMF values).

## 6 Illustration of OMI tropospheric NO<sub>2</sub> monitoring capabilities

Figure 7 shows a sequence of tropospheric NO<sub>2</sub> column observations over Europe from 15–18 October 2005. The figure illustrates that OMI is able to observe day-to-day variation in tropospheric NO<sub>2</sub> over northwestern Europe on days with limited cloud cover (cloud radiance <50%). On Sunday, 16 October 2005, a clear reduction of NO<sub>x</sub> pollution is observed over the Netherlands, Flanders and the Ruhr area, consistent with reduced Sunday-NO<sub>x</sub> emissions. This so-called weekend-effect has previously been reported by Beirle et al. (2003) after averaging many GOME observations, but appears directly observable from space with OMI.

As a further illustration of OMI's capabilities, Fig. 8 shows monthly averaged tropospheric NO<sub>2</sub> columns from OMI (left panel) and from SCIAMACHY (right panel) in August 2006 over Europe. This month was characterized by persistent cloud-cover for large areas in north-western Europe. We computed both monthly averages on a  $0.1^\circ \times 0.1^\circ$  grid and sampled whenever a cloud-free observation was available. The left panel shows that it was still possible to compute a monthly mean based on cloud-free OMI measurements. But SCIAMACHY – with less spatial and temporal coverage – did not record any cloud-free measurements over large parts of Europe during August 2006, so that many grid cells show up grey in the right panel of Fig. 8. Apart from the better spatial and temporal coverage, the OMI average also shows more spatial detail in the tropospheric NO<sub>2</sub> field. For instance, individual large cities including Madrid, Paris, and

**Table 3.** Contributions to the overall OMI tropospheric NO<sub>2</sub> retrieval error for individual, cloud-free pixels (cloud radiance fraction <50%) retrieved with the KNMI retrieval-assimilation-modelling approach (with the exception of the OMI standard product).  $\sigma_S$  is the uncertainty on the slant column,  $\sigma_{S_{st}}$  the uncertainty on the stratospheric slant column, and  $\sigma_{M_{tr}}$  the uncertainty on the tropospheric AMF.

| Instrument                 | Reference                              | $\sigma_S$                                   | $\sigma_{S_{st}}$                            | $\sigma_{M_{tr}}$      |
|----------------------------|--|--|--|------------------------|
| OMI near-real time product | This work                              | $0.70 \times 10^{15}$ molec cm <sup>-2</sup> | $0.15 \times 10^{15}$ molec cm <sup>-2</sup> | 10%–40%                |
| OMI standard product       | Bucsela et al. (2006) <sup>1</sup>     | $1.10 \times 10^{15}$ molec cm <sup>-2</sup> | $0.20 \times 10^{15}$ molec cm <sup>-2</sup> | not given <sup>2</sup> |
| SCIAMACHY                  | DeSmedt (2006),<br>Blond et al. (2007) | $0.47 \times 10^{15}$ molec cm <sup>-2</sup> | $0.25 \times 10^{15}$ molec cm <sup>-2</sup> | 10%–40%                |
| GOME                       | Boersma et al. (2004)                  | $0.45 \times 10^{15}$ molec cm <sup>-2</sup> | $0.25 \times 10^{15}$ molec cm <sup>-2</sup> | 15%–50%                |

<sup>1</sup>It is anticipated that improved lv1 calibration (due Spring 2007) and standard-product correction for spurious across-track variability will reduce the OMI standard product NO<sub>2</sub> slant column uncertainty.

<sup>2</sup>For “mostly clear” conditions, Bucsela (private communication, 2006) estimates 15–30% AMF uncertainty range.

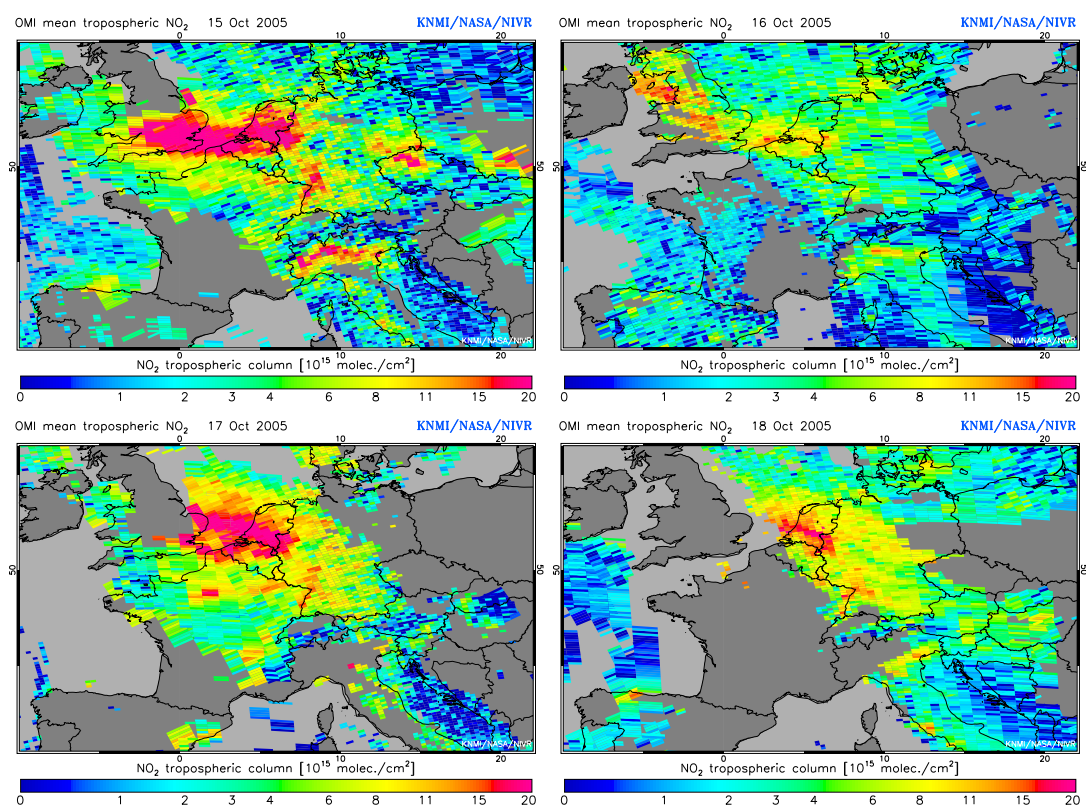


**Fig. 7.** OMI near-real time tropospheric NO<sub>2</sub> observed from Saturday, 15 October through Tuesday, 18 October 2005. Grey areas had cloud radiance fractions >50%. Daily images of OMI tropospheric NO<sub>2</sub> columns are provided at <http://www.temis.nl> in near-real time.

Moscow can be tracked down easily on the OMI map. Industrial regions such as the Po Valley, the Ruhr Area, and large parts of the UK also stand out.

## 7 Conclusions

The DOMINO near-real time algorithm retrieves tropospheric NO<sub>2</sub> columns from OMI within 3 h after measurement. This is possible with a new technique that is based on the assimilation of recently observed OMI NO<sub>2</sub> slant columns in the TM4 CTM. After the most recent observations have been digested by the assimilation scheme, TM4

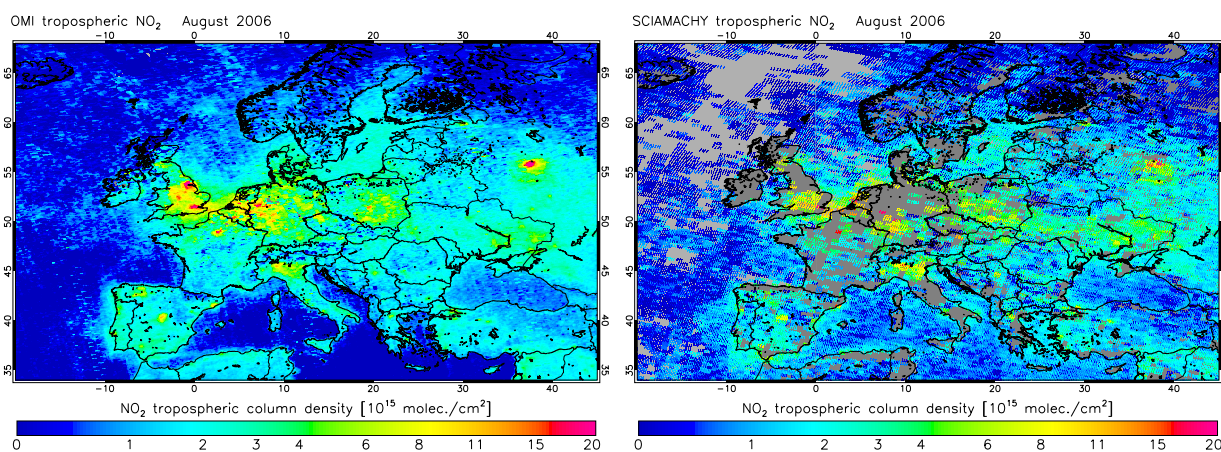


**Fig. 8.** Monthly mean tropospheric NO<sub>2</sub> column from OMI (left panel) and SCIAMACHY (right panel) for cloud-free (cloud radiance <50%) situations. Observations have been gridded at  $0.1^\circ \times 0.1^\circ$ . Grey grid cells have not been observed or had persistent cloud cover over August 2006.

is run forward in time with forecast ECMWF meteorological fields to predict the required retrieval inputs. Because of this, these inputs (stratospheric slant column, NO<sub>2</sub> and temperature profile) are available when a newly processed orbit of NO<sub>2</sub> and cloud data arrives at KNMI, and retrieval of tropospheric NO<sub>2</sub> columns is completed within a few minutes upon arrival of the data. We introduced a correction method for across-track variability associated with calibration errors in the OMI level 1b data that removes most of the spurious across-track variability. A simple statistical approach has been used to estimate the uncertainty in the slant columns. We find that the random error in the slant column is approximately  $0.70 \times 10^{15}$  molec cm<sup>-2</sup> for a single OMI observation.

From a comparison of SCIAMACHY cloud parameters retrieved by FRESCO from the O<sub>2</sub> A band, and OMI cloud parameters retrieved from the O<sub>2</sub>–O<sub>2</sub> absorption band at 477 nm, we find similar distributions of cloud fractions and cloud pressures. On average, SCIAMACHY cloud fractions are higher by 0.011 than OMI cloud fractions. OMI cloud pressures are approximately 60 hPa higher than FRESCO cloud pressures (for cloud fractions >0.05), consistent with different sensitivities of the two algorithms. The consistency between the SCIAMACHY and OMI cloud parameters, and the similar design and inputs for the NO<sub>2</sub> algorithms provide confidence in the OMI retrieval approach. OMI's unique capabilities for air quality monitoring are illustrated by a sequence of observations over Europe from 15–18 October 2005 showing day-to-day variability in air pollution, and a pronounced reduction in tropospheric NO<sub>2</sub> columns on Sunday 16 October 2005 related to the “weekend-effect”.

We expect that for NO<sub>2</sub> from OMI a new type of retrieval error becomes increasingly relevant. Forward model parameters, including a priori profile shapes, surface albedo's, and surface pressures, are currently obtained from data bases

with spatial resolutions much coarser than the actual spatial resolution of the retrieval. This is expected to lead to significant retrieval errors for some locations and times. We recommend detailed studies into the extent of these errors, and furthermore strongly encourage validation activities. Higher spatial resolution a priori information and models are needed for the full exploitation of the high resolution OMI data.

*Acknowledgements.* The near-real time retrieval was developed within the DOMINO project, “Derivation of Ozone Monitoring Instrument tropospheric NO<sub>2</sub> in near-real time”, funded by the NIVR and the Dutch User Support Programme, project code USP 4.2 DE-31. The authors would like to thank D. Schaub (EMPA) and J. de Haan for useful discussions. Thanks to the NASA SIPS for processing the slant column near-real time NO<sub>2</sub> and cloud data, and delivery to the KNMI system. I. DeSmedt and M. Van Roozendaal (BIRA) are kindly acknowledged for their retrievals of SCIAMACHY NO<sub>2</sub> slant columns.

Edited by: R. Cohen

## References

- Acarreta, J. R., De Haan, J. F., and Stammes, P.: Cloud pressure retrieval using the O<sub>2</sub>–O<sub>2</sub> absorption band at 477 nm, *J. Geophys. Res.*, 109, D05204, doi:10.1029/2003JD003915, 2004.
- Beirle, S., Platt, U., Wenig, M., and Wagner, T.: Weekly cycle of NO<sub>2</sub> by GOME measurements: A signature of anthropogenic sources, *Atmos. Chem. Phys.*, 3, 2225–2232, 2003, <http://www.atmos-chem-phys.net/3/2225/2003/>.
- Beirle, S., Platt, U., Wenig, M., and Wagner, T.: NO<sub>x</sub> production by lightning estimated with GOME, *Adv. Space Res.*, 34, 793–797, 2004.
- Beirle, S. N., Spichtinger, A., Stohl, K. L., Cummins, T., Turner, D., Boccippio, O. R., Cooper, M., Wenig, M., Grzegorski, U., Platt,

- U., and Wagner, T.: Estimating the NO<sub>x</sub> produced by lightning from GOME and NLDN data: a case study in the Gulf of Mexico, *Atmos. Chem. Phys.*, 6, 1075–1089, 2006, <http://www.atmos-chem-phys.net/6/1075/2006/>.
- Bergman, J. W. and Salby, M. L.: Diurnal Variations of Cloud Cover and Their Relationship to Climatological Conditions, *J. Climate*, 9, 2802–2820, 1996.
- Blond, N., Boersma, K. F., Eskes, H. J., van der A, R. J., Van Roozendaal, M., De Smedt, I., Bergametti, G., and Vautard, R.: Intercomparison of SCIAMACHY nitrogen dioxide observations, in-situ measurements and air quality modeling results over Western Europe, accepted, *J. Geophys. Res.*, 2007.
- Boersma, K. F., Bucsela, E. J., Brinksma, E. J., and Gleason, J. F.: NO<sub>2</sub>, in: OMI Algorithm Theoretical Basis Document, vol. 4, OMI Trace Gas Algorithms, ATB-OMI-04, Version 2.0, edited by: K. Chance, 13–36, NASA Distrib. Active Archive Cent., Greenbelt, Md., Aug., 2002.
- Boersma, K. F., Eskes, H. J., and Brinksma, E. J.: Error analysis for tropospheric NO<sub>2</sub> retrieval from space, *J. Geophys. Res.*, 109, D04311, doi:10.1029/2003JD003962, 2004.
- Boersma, K. F., Eskes, H. J., Meijer, E. W., and Kelder, H. M.: Estimates of lightning NO<sub>x</sub> production from GOME satellite observations, *Atmos. Phys. Chem.*, 5, 2311–2331, 2005.
- Bovensmann, H., Burrows, J. P., Buchwitz, M., Frerick, J., Noël, S., Rozanov, V. V., Chance, K. V., and Goede, A. P. H.: SCIAMACHY: Mission Objectives and Measurement Modes, *J. Atmos. Sci.*, 56(2), 127–150, 1999.
- Bregman, A., Segers, A. J., Krol, M., Meijer, E. W., and Van Velthoven, P. F.: On the use of mass-conserving wind fields in chemistry-transport models, *Atmos. Chem. Phys.*, 2, 447–457, 2003, <http://www.atmos-chem-phys.net/2/447/2003/>.
- Bucsela, E. J., Celarier, E. A., Wenig, M. O., Gleason, J. F., Veefkind, J. P., Boersma, K. F., and Brinksma, E. J.: Algorithm for NO<sub>2</sub> vertical column retrieval from the Ozone Monitoring Instrument, *IEEE Trans. on Geosci. Rem. Sens.*, 44(5), doi:10.1109/TGRS.2005.863715, 2006.
- Cede, A., Herman, J., Richter, A., Krotkov, N., and Burrows, J.: Measurements of nitrogen dioxide total column amounts using a Brewer double spectrophotometer in direct sun mode, *J. Geophys. Res.*, 111, D05304, doi:10.1029/2005JD006585, 2006.
- Dobber, M., Dirksen, R., Voors, R., Mount, G. H., and Levelt, P.: Ground-based zenith sky abundances and in situ gas cross sections for ozone and nitrogen dioxide with the Earth Observing System Aura Ozone Monitoring Instrument, *Appl. Opt.*, 44(14), 2846–2856, 2005.
- Dobber, M., Dirksen, R. P. F., Levelt, van den Oord, G. H. J., Voors, R. H. M., et al.: Ozone Monitoring Instrument Calibration, *IEEE Transactions on Geoscience and Remote Sensing*, 44(5), 1209–1238, doi:10.1109/TGRS.2006.869987, 2006.
- Eskes, H. J. and Boersma, K. F.: Averaging kernels for DOAS total-column satellite retrievals, *Atmos. Chem. Phys.*, 3, 1285–1291, 2003, <http://www.atmos-chem-phys.net/3/1285/2003/>.
- Eskes, H. J., van Velthoven, P. F. J., Valks, P., and Kelder, H. M.: Assimilation of GOME total ozone satellite observations in a three-dimensional tracer transport model, *Quart. J. Roy. Meteorol. Soc.*, 129, 1663, 2003.
- Fournier, N., Stammes, P., de Graaf, M., van der A, R., Piters, A., Grzegorski, M., and Kokhanovsky, A.: Improving cloud information over deserts from SCIAMACHY oxygen A-band measurements, *Atmos. Chem. Phys.*, 6, 163–172, 2006, <http://www.atmos-chem-phys.net/6/163/2006/>.
- Heland, J., Schlager, H., Richter, A., and Burrows, J. P.: First comparison of tropospheric NO<sub>2</sub> column densities retrieved from GOME measurements and in situ aircraft profile measurements, *Geophys. Res. Lett.*, 29, 44, doi:10.1029/2002GL015528, 2002.
- Herman, J. R. and Celarier, E. A.: Earth surface reflectivity climatology at 340–380 nm from TOMS data, *J. Geophys. Res.*, 102, 28 003–28 011, 1997.
- Houweling, S., Dentener, F. J., and Lelieveld, J.: The impact of nonmethane hydrocarbon compounds on tropospheric chemistry, *J. Geophys. Res.*, 103, 10 673–10 696, 1998.
- Jaeglé, L., Martin, R. V., Chance, K. V., Steinberger, L., Kurosu, T. P., Jacob, D. J., Modi, A. I., Yoboué, V., Sigha-Nkamdjou, L., Galy-Lacaux, C.: Satellite mapping of rain-induced nitric oxide emissions from soils, *J. Geophys. Res.*, 109, D21310, doi:10.1029/2004JD004787, 2004.
- Koelemeijer R. B. A., Stammes, P., Hovenier, J. W., and de Haan, J. F.: A fast method for retrieval of cloud parameters using oxygen A-band measurements from the Global Ozone Monitoring Instrument, *J. Geophys. Res.*, 106, 3475–3490, 2001.
- Koelemeijer, R. B. A., Stammes, P., Hovenier, J. W., and de Haan, J. F.: Global distributions of effective cloud fraction and cloud top derived from oxygen A band spectra measured by the Global Ozone Monitoring Experiment: Comparison to ISCCP data, *J. Geophys. Res.*, 107(D12), 4151, doi:10.1029/2001JD000840, 2002.
- Koelemeijer R. B. A., de Haan, J. F., and Stammes, P.: A database of spectral surface reflectivity in the range 335–772 nm derived from 5.5 years of GOME observations, *J. Geophys. Res.*, 108(D2), 4070, doi: 10.1029/2002JD002429, 2003.
- Konovalov, I. B., Beekmann, M., Vautard, R., Burrows, J. P., Richter, A., Nüß, H., and Elansky, N.: Comparison and evaluation of modelled and GOME derived tropospheric NO<sub>2</sub> columns over Western and Eastern Europe, *Atmos. Chem. Phys.*, 5, 169–190, 2005, <http://www.atmos-chem-phys.net/5/169/2005/>.
- Krotkov, N. A., Carn, S. A., Krueger, A. J., Bhartia, P. K., and Yang, K.: Band residual difference algorithm for retrieval of SO<sub>2</sub> from the AURA Ozone Monitoring Instrument (OMI), *IEEE Trans. Geosci. Remote Sensing, AURA Special Issue*, 44(5), 1259–1266, 2006.
- Kurosu, T. P., Chance, K., and Sioris, C. E.: Preliminary Results for HCHO and BrO from the Eos-Aura Ozone Monitoring Instrument, *Proc. of SPIE*, Vol. 5652, 116–123, 2005.
- Lauer, A., Dameris, M., Richter, A., and Burrows, J. P.: Tropospheric NO<sub>2</sub> columns: a comparison between model and retrieved data from GOME measurements, *Atmos. Chem. Phys.*, 2, 67–78, 2002, <http://www.atmos-chem-phys.net/2/67/2002/>.
- Leue, C., Wenig, M., Wagner, T., Klimm, O., Platt, U., and Jähne, B.: Quantitative analysis of NO<sub>x</sub> emissions from GOME satellite image sequences, *J. Geophys. Res.*, 106, 5493–5505, 2001.
- Levelt, P. F., van den Oord, G. H. J., Dobber, M. R., Mälkki, A., Visser, H., de Vries, J., Stammes, P., Lundell, J. O. V., and Saari, H.: The Ozone Monitoring Instrument, *IEEE Trans. on Geosci. Rem. Sens.*, 44(5), doi:10.1109/TGRS.2006.872333, 2006a.

- Levelt, P. F., Hilsenrath, E., Leppelmeier, G. W., van den Oord, G. H. J., Bhartia, P. K., Tamminen, J., de Haan, J. F., and Veefkind, J. P.: Science Objectives of the Ozone Monitoring Instrument, *IEEE Trans. on Geosci. Rem. Sens.*, 44(5), doi:10.1109/TGRS.2006.872336, 2006b.
- Ma, J., Richter, A., Burrows, J. P., Nüß, H., and van Aardenne, J. A.: Comparison of model-simulated tropospheric NO<sub>2</sub> over China with GOME-satellite data, *Atmos. Environ.*, 40, 593–604, 2006.
- Martin, R. V., Jacob, D. J., Chance, K. V., Kurosu, T. P., Palmer, P. I., and Evans, M. J.: Global inventory of Nitrogen Dioxide Emissions Constrained by Space-based Observations of NO<sub>2</sub> Columns, *J. Geophys. Res.*, 108, 4537, doi:10.1029/2003JD003453, 2003.
- Martin, R. V., Parrish, D. D., Ryerson, T. B., Nicks Jr., D. K., Chance, K., Kurosu, T. P., Jacob, D. J., Sturges, E. D., Fried, A., and Wert, B. P.: Evaluation of GOME satellite measurements of tropospheric NO<sub>2</sub> and HCHO using regional data from aircraft campaigns in the southeastern United States, *J. Geophys. Res.*, 109(D24), D24307, doi:10.1029/2004JD004869, 2004.
- Martin, R. V., Sioris, C. E., Chance, K., Ryerson, T. B., Bertram, T. H., Wooldridge, P. J., Cohen, R. C., Neuman, J. A., Swanson, A., and Flocke, F. M.: Evaluation of space-based constraints on global nitrogen oxide emissions with regional aircraft measurements over and downwind of eastern North America, *J. Geophys. Res.*, 111, D15308, doi:10.1029/2005JD006680, 2006.
- Olivier, J., Peters, J., Granier, C., Pétron, G., Müller, J.-F., and Wal lens, S.: Present and future surface emissions of atmospheric compounds, POET report #2, EU project EVK2-1999-00011, 2003.
- van den Oord, G. H. J., Rozemeijer, N. C., Schenkelaars, V., Levelt, P. F., Dobber, M. R., Voors, R. H. M., Claas, J., ter Linden, M., de Haan, C., van de Berg, T.: OMI Level 0 to 1b Processing and Operational Aspects, *IEEE Trans. on Geosci. Rem. Sens.*, 44(5), doi:10.1109/TGRS.2006.872935, 2006.
- Ordóñez, C., Richter, A., Steinbacher, M., Zellweger, C., Nüß, H., J., Burrows, P., and Prévôt, A. S. H. (2006): Comparison of 7 years of satellite-borne and ground-based tropospheric NO<sub>2</sub> measurements around Milan, Italy, *J. Geophys. Res.*, 111, D05310, doi:10.1029/2005JD006305, 2006.
- Petritoli, A., Bonasoni, P., Giovanelli, G., et al.: First comparison between ground-based and satellite-borne measurements of tropospheric nitrogen dioxide in the Po basin, *J. Geophys. Res.*, 109, D15307, doi:10.1029/2004JD004547, 2004.
- Petritoli, A., Palazzi, E., Volta, C., and Giovanelli, G.: Validation of NO<sub>2</sub> tropospheric columns from space in the Po Valley (Italy), in: *Tropospheric sounding from space, ACCENT-TROPOSAT-2 in 2004-5*, edited by: Burrows, J. P. and Borrell, P., 308–312, 2005.
- Platt, U.: Differential Optical Absorption Spectroscopy (DOAS), in: *Air monitoring by Spectroscopic Techniques*, edited by: Sigrist, M. W., *Chemical Analysis*, 127, 27–76, 1994.
- Richter, A., Burrows, J. P., Nüß, H., Granier, C., and Niemeier, U.: Increase in tropospheric nitrogen dioxide over China observed from space, *Nature*, 437, 129–132, doi:10.1038/nature04092, 2005.
- Riishøjgaard, L. P.: A direct way of specifying flow-dependent background error correlations for meteorological analysis systems, *Tellus A*, 50, 42–57, doi:10.1034/j.1600-0870.1998.00004.x, 1998.
- Savage, N. H., Law, K. S., Pyle, J. A., Richter, A., Nüß, H., and Burrows, J. P.: Using GOME NO<sub>2</sub> satellite data to examine regional differences in TOMCAT model performance, *Atmos. Chem. Phys.*, 4, 1895–1912, 2004, <http://www.atmos-chem-phys.net/4/1895/2004/>.
- Schaub, D., Boersma, K. F., Kaiser, J. W., Weiss, A. K., Folini, D., Eskes, H. J., and Buchmann, B.: Comparison of GOME tropospheric NO<sub>2</sub> columns with NO<sub>2</sub> profiles deduced from ground-based in situ measurements, *Atmos. Chem. Phys.*, 6, 3211–3229, 2006, <http://www.atmos-chem-phys.net/6/3211/2006/>.
- Schaub, D., Boersma, K. F., Keller, J., Folini, D., Brunner, D., Buchmann, B., Berresheim, H., and Staehelin, J.: SCIAMACHY tropospheric NO<sub>2</sub> over the Alpine region and importance of pixel surface pressure for the column retrieval, *Atmos. Chem. Phys. Discuss.*, 7, 429–468, 2007, <http://www.atmos-chem-phys-discuss.net/7/429/2007/>.
- Stammes, P.: Spectral radiance modeling in the UV-Visible range, IRS2000: in: *Current problems in atmospheric radiation*, edited by: Smith, W. L. and Timofeyev, Y. J., 385–388, A. Deepak, Hampton, Va, USA, 2000.
- Vandaele, A. C., Hermans, C. P., Simon, C., Carleer, M., Colin, R., Fally, S., Merienne, M. F., Jenouvrier, A., and Coquart, B.: Measurements of the NO<sub>2</sub> absorption cross-section from 42 000 cm<sup>-1</sup> to 10 000 cm<sup>-1</sup> (238–1000 nm) at 220 K and 294 K, *J. Quant. Spectrosc. Radiat. Transfer*, 59, 171–184, 1998.
- van der A, R. J., Peters, D. H. M. U., Eskes, H. J., Boersma, K. F., Van Roozendaal, M., De Smedt, I., and Kelder, H. M.: Detection of the trend and seasonal variation in tropospheric NO<sub>2</sub> over China, *J. Geophys. Res.*, 111, D12317, doi:10.1029/2005JD006594, 2006.
- van Noije, T. P. C., Eskes, H. J., Dentener, F. J., Stevenson, D. S., Ellingsen, K., et al.: Multi-model ensemble simulations of tropospheric NO<sub>2</sub> compared with GOME retrievals for the year 2000, *Atmos. Chem. Phys.*, 6, 2943–2979, 2006, <http://www.atmos-chem-phys.net/6/2943/2006/>.
- Veefkind, J. P. and de Haan, J. F.: DOAS total O<sub>3</sub> algorithm, in: *OMI Algorithm Theoretical Basis Document, vol. 2, OMI Ozone Product, ATB-OMI-02, Version 2.0*, edited by: P. K. Bhartia, NASA Distrib. Active Archive Cent., Greenbelt, Md., Aug. 2002.
- Velders, G. J. M., Granier, C., Portmann, R. W., Pfeilsticker, K., Wenig, M., Wagner, T., Platt, U., Richter, A., and Burrows, J. P.: Global tropospheric NO<sub>2</sub> column distributions: Comparing 3-D model calculations with GOME measurements, *J. Geophys. Res.*, 106, 12 643–12 660, 2001.
- Voors, R., Dobber, M., Dirksen, R., and Levelt, P.: Method of calibration to correct for cloud-induced wavelength shifts in the Aura satellites Ozone Monitoring Instrument, *Appl. Opt.*, 45(15), 3652–3658, 2006.
- Wang, P., Stammes, P., and Fournier, N.: Test and first validation of FRESCO+, *Proceedings of SPIE*, 6362 pp., 13–20, *Remote Sensing of Clouds and the Atmosphere XI*, edited by: Slusser, R., Schäfer, K., and Camerón, A., 2006.
- WMO: Annual Report, Bass, Johnsten, 1975.